Braz J Phys (2013) 43:13–21
DOI 10.1007/s13538-013-0120-7

CONDENSED MATTER

Temperature-Dependent Current–Voltage (I–V) and Capacitance–Voltage (C–V) Characteristics of Ni/Cu/n-InP Schottky Barrier Diodes

Y. Munikrishana Reddy · M. K. Nagaraj · M. Siva Pratap Reddy · Jung-Hee Lee · V. Rajagopal Reddy

Received: 24 October 2011 / Published online: 27 February 2013

Abstract The current-voltage (I–V) and capacitance-voltage (C–V) characteristics of Ni/Cu/n-InP Schottky barrier diodes are studied over a wide temperature range, from 210 K to 420 K. The I–V characteristics display anomalous thermal behavior. The apparent barrier height decays, and the ideality factor grows at low temperatures, and the series resistances resulting from Cheung's and Norde's procedures are markedly temperature dependent. The nonlinearity of the Richardson plot and the strong temperature dependence of the Schottky-barrier parameters indicate that the interface is spatially inhomogeneous. Plots of the zero-bias barrier height as a function of 1/(2kT) points to a Gaussian distribution of barrier heights with 0.90 eV mean height and 0.014 eV standard deviation. When this distribution is accounted for, a Richardson of 6.5 A/(cm K)^2 results, relatively close to the 9.4/(cm K)^2 predicted by theory. We conclude that, combined with a Gaussian distribution of barrier heights, the thermionic-emission mechanism explains the temperature-dependent I–V and C–V characteristics of the studied Schottky-barrier diodes.

Keywords Ni/Cu/n-InP Schottky diode · Ideality factor · Gaussian distribution · Barrier inhomogeneities

Y. Munikrishana Reddy · M. K. Nagaraj
S.S.B.N. Degree & P.G. College, Anantapur 515 001, India

M. Siva Pratap Reddy (✉) · J.-H. Lee
School of Electrical Engineering and Computer Science,
Kyungpook National University, Daegu 702-201, South Korea
e-mail: dr.mspreddy@gmail.com

V. Rajagopal Reddy
Department of Physics, Sri Venkateswara University,
Tirupati 517 502, India

1 Introduction

Indium phosphide substrate semiconductors exhibit high electron mobilities, large direct band gaps, high saturation velocities, and large breakdown voltages, properties that would favor the development of high-speed metal–semiconductor field-effect transistors [1], electro-optical devices [2], and laser diodes [3]. Nonetheless, the relatively small Schottky barrier heights [4] at metal–semiconductor (MS) interfaces restrict their application to low-barrier Schottky-barrier diodes (SBDs), which are valuable as infrared detectors in cryogenic engineering and as sensors in thermal imaging [5, 6]. Motivated by practical and scientific considerations, we are therefore interested in the transport properties of such diodes. Given the envisioned applications, however, it is clearly insufficient to analyze their current–voltage (I–V) characteristics at room temperature.

Electrical conduction mechanisms and technological aspects of MS structures have been examined by Rhoderick [7] and Rideout [8]. Conduction in MS junctions is primarily due to majority carriers, in contrast with transport in p–n junctions, in which the minority carriers play a central role. The technological importance of MS Schottky contacts has drawn much attention to their current–voltage (I–V) and capacitance–voltage (C–V) characteristics are of great interest [9, 10]. Although the temperature-dependent electrical properties of Schottky diodes have been intensively studied, both theoretically and experimentally [11–13], the low temperature behavior is only partially understood. The strong thermal dependences of barrier heights and ideality factors yield nonlinear Richardson plots in disagreement with thermionic emission (TE) theory [14–17]. Also puzzling are the nonlinear $\ln(I_o/T^2)$ vs. 10^3/T plots, from the slope of which the activation energy is obtained in TE theory.

The nonlinearities indicate that the MS interface barriers are inhomogeneous. Although clear identification of the mechanisms responsible for the inhomogeneities is still missing, it seems safe to assume that the barrier height depends on the atomic structure at the interface. Among the possible sources of inhomogeneity are therefore grain boundaries, multiple phases, facets, defects, and the coexistence of different phases [18–21].

The temperature-dependent characteristics of Schottky contacts on n-type InP have received considerable attention [22–26]. Cetin et al. [22] studied the temperature dependence of the I–V characteristics of Au/InP SBD's and found ideality factors that decrease, while the barrier heights increase, upon warming. Cimilli et al. [23] reported the I–V characteristics of an Ag/n-InP SBD, which pointed to inhomogeneous Schottky barrier heights in the temperature range 30–320 K, the barrier height and ideality factor varying from 0.20 eV and 3.89 at 70 K to 0.61 eV and 1.18 at 320 K, respectively. The I–V and C–V characteristics of the same junction were studied by Soylu et al. [24] in the 60–300 K range. The ideality factor of the diode drops, while the zero-bias Schottky barrier height rises, as a function of temperature. From the I–V–T and C–V–T characteristics of another junction, Ni/Au SBD's. Naik et al. [25] found barrier parameters that vary significantly with temperature. More recently, Reddy et al. [26] discussed the temperature-dependent I–V characteristics of a Pt/Ti/n-InP Schottky diode in the temperature range 200–440 K to show that the experimental data are consistent with a gaussian distribution of barrier heights. From the estimated mean value and standard deviation, they inferred that the inhomogeneity is due to potential fluctuations at the interface.

Here, we present a similar analysis of the forward bias I–V and reverse bias C–V characteristics of Ni/Cu/n-InP SBD's in the 210–420 K temperature range. The study is analogous to the work reported in [26]. We show that the I–V characteristics have anomalous thermal dependence at low temperatures and demonstrate that this deviation from TE theory is quantitatively consistent with a random distribution of barrier heights. Additional evidence in favor of this interpretation is obtained when the barrier heights obtained from the I–V characteristics are compared with those extracted from the C–V characteristics.

2 Experimental Technique

The wafers in our study are liquid-encapsulated czochralski (LEC)-grown undoped n-InP (100) 2 μm thick with carrier concentrations in the $4.9–5\times10^{15}$ cm^{-3} range. The wafers were initially degreased with three organic solvents—trichloroethylene, acetone, and methanol—by means of 5-min ultrasonic in each step, to remove contaminants. They were subsequently rinsed in deionized water, dried in N_2 flow, and etched with HF (49 %)/H_2O (1:10) to remove oxides from the substrate. Ohmic contacts with 500 Å thickness is formed by indium evaporation at 6×10^{-6} mbar pressure on the rough side of each InP wafer. The wafers were then annealed in a rapid thermal annealing system at 350 °C for 1 min in high purity N_2 ambient. Immediately after that, they were inserted in the e-beam evaporation chamber. To form the Schottky contacts, metallic Cu (200 Å) and Ni (300 Å) were evaporated through a stainless steel mask with 0.7 mm diameter. The metal layer thicknesses and the deposition rates, between 0.2 and 1 Å/s, were monitored with a digital quartz thickness monitor (model DTM-10). The I–V and C–V characteristics of the Cu/Ni/n-InP SBDs were measured in the range of 210–420 K in steps of 30 K with a Keithley 2400 and DLS-83D spectrometer. The device temperature was controlled to ±1 K accuracy by a thermal controller DLS-83D-1 cryostat.

3 Results and Discussion

3.1 Current–Voltage Characteristics

The techniques allowing measurement of MS barrier heights can divided into four categories: current–voltage, activation–energy, capacitance–voltage, and photoelectric methods. Our procedure belongs to the first, most widely used category [7]. Figure 1 shows the semi-log forward and reverse bias I–V characteristics of Ni/Cu/n-InP SBD in the 210–420 K temperature range. As the temperature rises, the parameters of the Ni/Cu/n-InP SBD extracted from the curves show well-defined trends. The leakage current at −1 V increases from 2.76×10^{-8} to 1.98×10^{-3} A. In an ideal SBD, the forward-bias

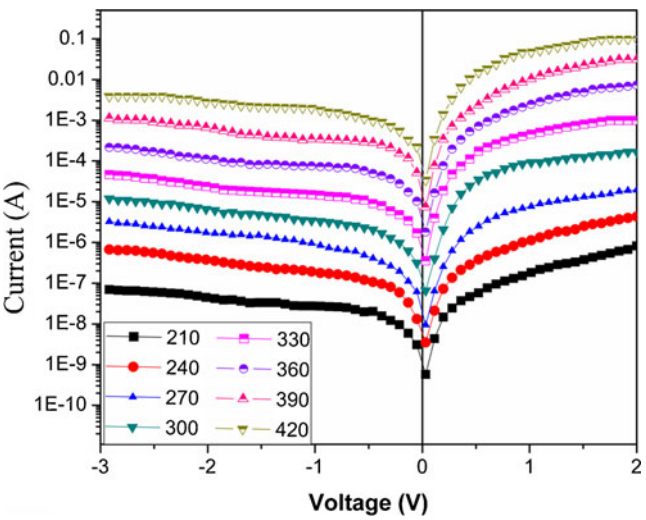

Fig. 1 Current–voltage characteristics of Ni/Cu/n-InP SBDs at various temperatures

current, due to thermo-electric conduction, would be given by the expression [9]

$$I = I_o \exp\left(\frac{q(V - \mathrm{IR_s})}{\mathrm{nkT}}\right)\left[1 - \exp\left(\frac{-q(V - \mathrm{IR_s})}{\mathrm{kT}}\right)\right] \quad (1)$$

with n=1. Here, R_S is the barrier resistance and the pre-factor defining the reverse bias saturation current is

$$I_o = AA^* T^2 \exp\left(\frac{-q\Phi_{bo}}{kT}\right) \quad (2)$$

where q is the electronic charge, Φ_{bo} is the zero-bias height, A is the diode area, and A^* is the effective Richardson constant. For n-InP, the effective electronic mass is m^*=0.078m_0, where m_0 is the rest mass, and it results that A^*=9.4 A/(cm K)^2.

Equation (1) brings out the physics in I–V characteristics, such as the ones in Fig. 1. Consider, for instance, the forward-bias portion of those plots. In the zero-bias regime, the ratio q(V-IR$_S$)/kT is very small, and the right-hand side of Eq. (1) is a linear function of the voltage. As the bias grows, the second term within square brackets on the right-hand side of Eq. (1) becomes negligible and the device enters the nonlinear regime. Initially, the current is so small that the voltage drop due to the barrier resistance, R_S, i.e., the term IR$_S$ within each of the two parentheses on the right-hand side of Eq. (1), can be neglected. Governed by thermal activation, the current now grows exponentially with the applied voltage, so that ln(I) vs. V plots, such as those depicted in Fig. 1, are expected to follow straight lines.

The current rises much faster than the voltage in this exponential growth regime. For sufficiently high bias, therefore, the potential drop IR$_S$ becomes comparable to V, the growth is curbed, and the ln(I) vs. V plots show negative curvature as the device progresses towards a quasi-Ohmic regime in which the current must be approximately proportional to the applied bias, to make the effective bias V–IR$_S$ in the numerator of the first exponent on the right-hand side of Eq. (1) nearly constant, i.e., to insure that the effective bias grow only logarithmically with the applied bias. As the forward-bias curves in Fig. 1 show, the exponential growth, the negative curvature, and the quasi-Ohmic regime are easily identified in experimental data. The temperature dependence of the exponential rise is nonetheless poorly described by Eq. (1) with n=1.

To improve the agreement with Eq. (1), it has become traditional to release the constraint n=1 and let n be an empirical parameter. The *ideality factor* n can be obtained from the slope of the straight line in the exponential growth region of the forward-bias ln(I) vs. V plot by means of the following relation:

$$n = \frac{q}{kT}\left(\frac{dV}{d\ln I}\right) \quad (3)$$

Applied to our data, this analysis yields the SBH Φ_{bo}= 0.52 eV and the ideality factor n=3.31 at 210 K, and Φ_{bo}= 0.70 eV and n=1.47 at 420 K. Figure 2 shows that Φ_{bo} decays monotonically while the ideality factor grows, also monotonically, as the temperature is reduced. There is clear deviation from the ideal TE model.

Ideality factors substantially larger than unity are usually due to secondary characteristics of the interface, such as lateral inhomogeneities of the barrier height created by interface defects. A distribution of barrier heights affects the temperature dependence of the I–V characteristics, because the electrons are able to surmount the lower barriers even at relatively low temperatures [24–26]. At such temperatures, therefore, current transport will be dominated by the flow through the low-barrier patches, and depending on the distribution function, the effective barrier height—the average height of the barriers allowing conduction—may be a small fraction of Φ_{bo}. And the effective bias, that is, the bias necessary to defeat the effective barrier height, is smaller than V, a reduction that is mathematically equivalent to an enhancement of the ideality factor. As the temperature rises, more and more electrons have sufficient energy to overcome the higher barriers, and the effective barrier height comes closer to Φ_{bo}, while the ideality factor comes closer to unity. Non-uniform thicknesses and interfacial charges are among the defects that can introduce barrier inhomogeneities.

The barrier height can alternatively be obtained from the temperature dependence of the saturation current. This becomes evident when Eq. (2) is rewritten in the form

$$\ln\left(\frac{I_o}{T^2}\right) = \ln(AA^*) - \frac{q\Phi_{bo}}{kT} \quad (4)$$

The plot of ln(I_o/T^2) versus 10^3/T, known as the conventional Richardson plot, is therefore expected to be linear. As Fig. 3 shows, however, only above 250 K do our experimental

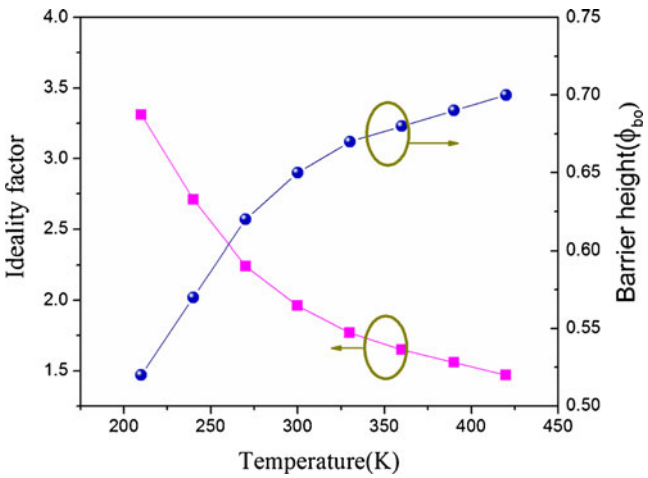

Fig. 2 The difference between ideality factor and barrier height in Ni/Cu/n-InP SBDs at different temperatures

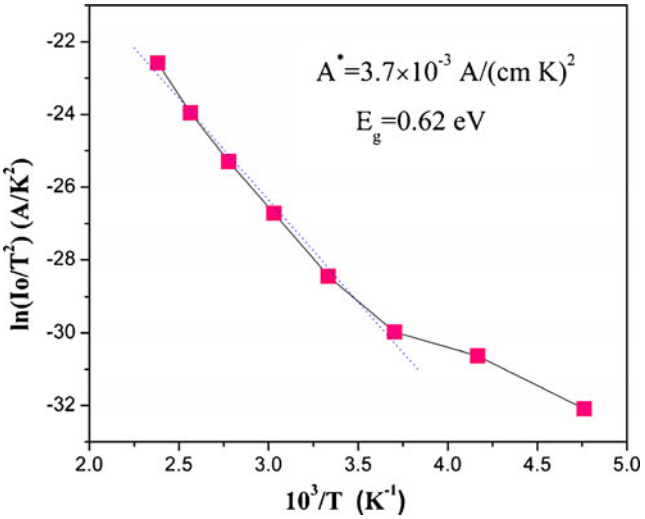

Fig. 3 Richardson plot of $\ln(I_o/T^2)$ versus 10^3/T for Ni/Cu/n-InP SBD

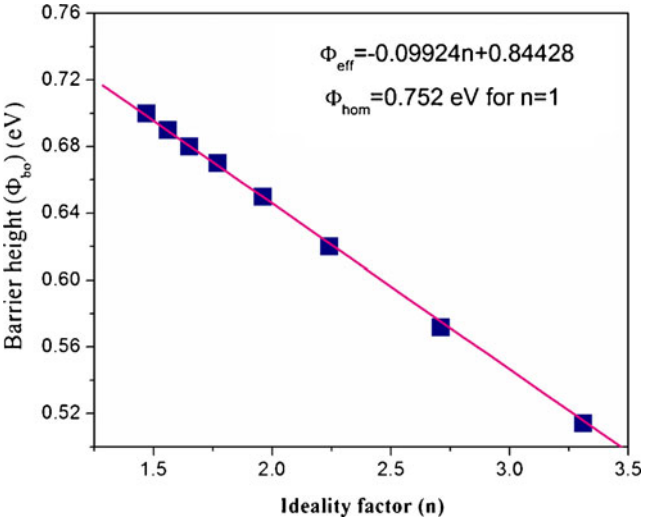

Fig. 4 The zero-bias barrier height versus ideality factor for the Ni/Cu/n-InP SBDs

points follow a straight line, at temperatures associated with relatively small ideality factors and relatively large barrier heights. Similar results have been reported by several authors [22–26]. From the slope of the dotted line in Fig. 3, an activation energy of 0.62 eV is obtained. From the ordinate intercept, we find $A^*=3.7\times10^{-3}$ A/(cm K)^2, surprisingly lower than the calculated value of 9.4 A/(cm K)^2. The bowing in the Richardson plot also points to spatially inhomogeneous barrier heights, i.e., to an interface consistent of low- and high-barrier areas [14–17, 27–29]. A laterally inhomogeneous barrier may even lead to temperature-dependent A^* in Eq. (4), as shown by Horvath [30].

Schmitsdorf et al. [31, 32] have proved that Tung's pinch-off model [12] leads to a linear relation between the experimental zero-bias barrier height and the ideality factor. That this result agrees remarkably well with our data is shown by the least-square fit in Fig. 4. Extrapolated to $n=1$, the straight line yields an ideal barrier height of approximately 0.752 eV. The measured heights are smaller because the barrier is inhomogeneous and the higher-barrier patches are frozen out of conduction at low temperatures.

The series resistance R_S can be computed by two different procedures, both due to Cheung and Cheung [33], applied to the forward-bias I–V characteristics beyond the exponential growth range. Equation (1) then takes the simpler form

$$I = I_o \exp\left[\frac{q(V - \mathrm{IR_S})}{\mathrm{nkT}}\right] \tag{5}$$

From Eq. (5), two equalities can be derived, each of which determines R_S:

$$\frac{dV}{d\ln(I)} = \mathrm{IR_S} + n\left(\frac{\mathrm{kT}}{\mathrm{q}}\right) \tag{6}$$

and

$$H(I) = V - n\left(\frac{\mathrm{kT}}{q}\right)\ln\left(\frac{I}{\mathrm{AA^*T^2}}\right) \tag{7}$$

where $H(I)$ is defined by the equality:

$$H(I) = \mathrm{IR_S} + n\Phi_{\mathrm{bo}} \tag{8}$$

Figures 5a and b plots dV/dlnI and $H(I)$ versus I, respectively, measured at the eight temperatures in our experiment. Equation (6) predicts a straight line in the R_S-dominant voltage range, i.e., for voltages beyond the exponential growth range, such that the second term within the parentheses in the exponent on the right-hand side of Eq. (5) becomes non-negligible and the I–V characteristics in Fig. 1 acquire negative curvature. According to Eq. (6), the slope of the straight line is R_S and the y-intercept is nkT/q.

Once the ideality factor is determined from Eq. (6), the right-hand side of Eq. (7) can be computed from the currents and bias voltages measured in the R_S-dominant regime. Figure 5b plots H(I) as function of the current at each temperature over a broader current range. According to Eq. (8), each plot should be a straight-line with y-axis intercept $n\Phi_{\mathrm{bo}}$. The slope should be equal to R_S and can checked against the series resistances obtained from Fig. 5a to check the consistency of Cheung's approach. Table 1 shows that the series resistances obtained from the $H(I)$ vs. I and the dV/dlnI vs. I plots are in good agreement at each temperature.

Also tabulated are the barrier heights and ideality factors obtained from Eqs. (6) and (8), respectively. As the temperature rises from 210 to 420 K, the ideality factors decrease from 4.01 to 1.75, the barriers grow from 0.56 to 0.73 eV, and the arithmetic averages between the two values for R_S at each temperature decay from 959 to 85 Ω. While the barrier

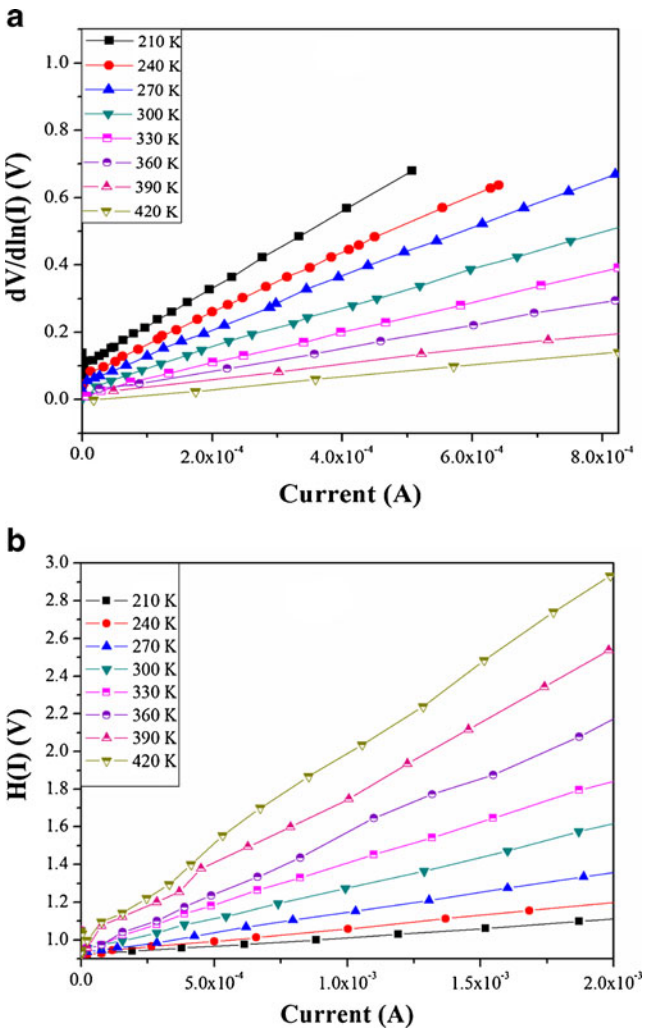

Fig. 5 Cheung's plots of **a** dV/dln(I) versus I and **b** H(I) versus I for Ni/Cu/n-InP SBDs

heights in the table, obtained from the downward curvature region of the forward-bias I–V plots in Fig. 1, agree well with the barrier heights in Fig. 2, obtained from the exponential growth region of the same I–V characteristics, there is significant difference between the n's in Table 1 and in Fig. 2. This discrepancy indicates that the ideality factor is bias dependent, i.e., it changes with the voltage drop across the interfacial layer, presumably because the charge of the interface states is a function of the bias [34].

Norde [35] proposed yet another method to determine R_S when TE is dominant. While Cheung's methods cover only the region of the forward bias I–V plots characterized by non-exponential growth, Norde's procedure covers the entire forward-bias region of I–V plots. Norde defined the function

$$F(V) = \frac{V}{2} - \frac{kT}{q}\ln\left(\frac{I(V)}{AA^*T^2}\right) \tag{9}$$

where $I(V)$ is the current obtained from the experimental I–V curve.

The function $F(V)$ is expected to first decrease and then increase as the bias voltage rises from the linear into the nonlinear regime. Accordingly, in Fig. 6, the plot of $F(V)$ as a function of V for our diode shows a clear minimum at each temperature. If $V_{\min}$ is the bias at the minimum, then the barrier height is given by the following expression [35]

$$\Phi_{\mathrm{bo}}^{\mathrm{Norde}} = F(V_{\min}) + \frac{V_{\min}}{2} - \frac{\mathrm{kT}}{q} \tag{10}$$

For non-ideal contacts (n>1), the series resistance R_S is given by the expression

$$R_s = \frac{kT}{qI_{\min}}(2-n) \tag{11}$$

where q is the charge and $I_{\min}$ is the current at the bias voltage $V_{\min}$.

The series resistances extracted from the Norde's plot, ranging from 1,602 Ω at 210 K to 184 Ω at 420 K, are listed in Table 2. The R_S are also plotted as a function of the temperature in Fig. 7, which compares them with the somewhat smaller series resistances obtained from Fig. 6. We have no explanation for the distances separating the squares from the circles and inverted triangles in Fig. 7, but note that similar

Table 1 Series resistance, ideality factor and barrier height values extracted with corresponding voltages from forward bias I–V characteristics by Cheung's method of the Ni/Cu/n-InP SBDs in the temperature range 210–420 K

T(K)	dV/dlnI			*H(I)*		
	Range (V)	R_S (Ω)	n	Range (V)	R_S (Ω)	$\Phi_{bo}^{H(I)}$(eV)
210	0.0985–0.6425	942	4.01	0.9251–1.512	976	0.56
240	0.0861–0.6832	745	3.67	0.9385–1.706	777	0.62
270	0.0527–0.7476	570	3.32	0.9457–1.942	599	0.65
300	0.0297–0.5864	422	2.94	0.9581–2.507	451	0.68
330	0.0173–0.4308	303	2.61	0.9666–2.864	331	0.70
360	0.0166–0.3222	189	2.35	0.9782–3.394	215	0.71
390	0.0157–0.1937	116	2.06	0.9885–3.535	133	0.72
420	0.0051–0.1562	78	1.75	1.0351–3.616	92	0.73

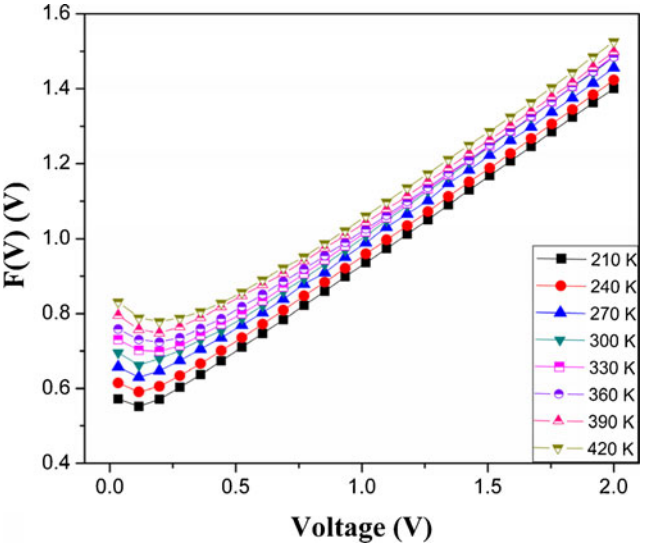

Fig. 6 $F(V)-V$ plots for Ni/Cu/n-InP SBDs at various temperatures

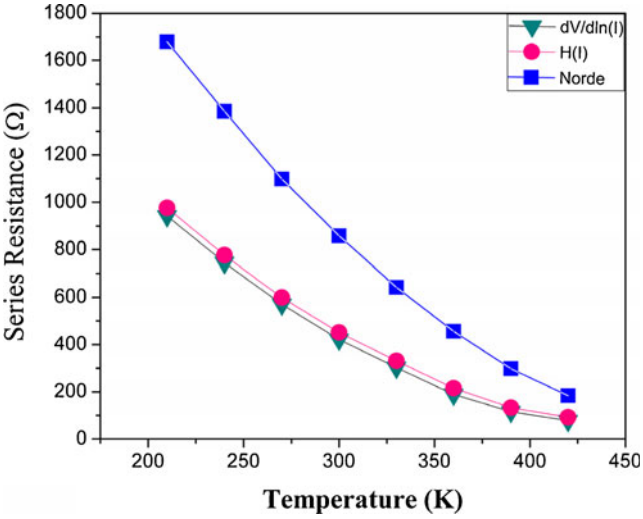

Fig. 7 Temperature dependence of the series resistances obtained from various methods for Ni/Cu/n-InP SBDs

discrepancies between series resistances obtained from Cheung's and from Norde's procedures have often been reported in the literature.

Whether calculated by Cheung's or Norde's methods, the series resistance decreases markedly as the diode is heated. The decay may be due to mechanisms responsible for the temperature dependence of the ideality factor, but it has been suggested that the large low-temperature resistances may reflect a reduction in free-carrier concentration [36].

3.2 Inhomogeneous Barrier Analysis

The abnormal behavior of the I–V characteristics of SBDs has been attributed to barrier height inhomogeneity. This inhomogeneity can be modeled by a Gaussian distribution $P(\Phi_{bo})$ of barrier heights, with mean value $\overline{\Phi}_{bo}$ and standard deviation σ_o, represented by the expression [7, 37]:

Table 2 Temperature dependent values of various experimental parameters obtained from I–V and C–V measurements of the Ni/Cu/n-InP SBDs

T (K)	I–V n	Φ_{bo}^{I-V} (eV)	Φ_{bo}^{C-V} (eV)	Norde (Ω)
210	3.31	0.52	0.78	1,602
240	2.71	0.57	0.75	1,415
270	2.24	0.62	0.72	1,139
300	1.96	0.65	0.70	982
330	1.77	0.67	0.68	642
360	1.65	0.68	0.66	546
390	1.56	0.69	0.64	298
420	1.47	0.70	0.63	184

$$P(\Phi_{bo}) = \frac{1}{\sigma_S\sqrt{2\pi}} \exp\left[-\frac{(\Phi_{bo}-\overline{\Phi}_{bo})^2}{2\sigma_o^2}\right] \tag{12}$$

The current across a Schottky diode with barrier inhomogeneity is then given by the integral [28]

$$I(V) = \int_{-\infty}^{+\infty} I(\Phi_{bo}, V)P(\Phi_{bo})d\Phi \tag{13}$$

where $I(\Phi_{bo},V)$ is the current across a barrier height Φ_{bo} at bias voltage V, computed from ideal TE theory.

Equation (13) yields the following result for the total current at forward bias V [9]:

$$I(V) = AA^*T^2 \exp\left[-\frac{q}{kT}\left(\overline{\Phi}_{bo} - \frac{q\sigma_o^2}{2kT}\right)\right] \times \exp\left(\frac{qV}{n_{ap}kT}\right)\left[1-\exp\left(-\frac{qV}{kT}\right)\right] \tag{14}$$

with

$$I_o = AA^*T^2 \exp\left(-\frac{q\Phi_{ap}}{kT}\right) \tag{15}$$

where n_{ap} and Φ_{ap} are the apparent ideality factor and barrier height, respectively. The apparent barrier height is given by the equality

$$\Phi_{ap} = \overline{\Phi}_{bo}(T=0) - \frac{q\sigma_o^2}{2kT} \tag{16}$$

In the ideal case (n=1), the following expression can be obtained:

$$\left(\frac{1}{n_{ap}} - 1\right) = -\rho_2 + \frac{q\rho_3}{2kT} \tag{17}$$

The Gaussian parameters $\overline{\Phi}_{bo}$ and σ_o are linear functions of the bias, i.e., $\overline{\Phi}_b = \overline{\Phi}_{bo} + \rho_2 V$ and $\sigma_o = \sigma_o + \rho_3 V$, where the coefficients ρ_2 and ρ_3, which may be temperature dependent, quantify the deformation of the barrier height under a bias voltage. The typically small temperature dependence of σ_o has often been neglected [28]. Section 3.3 will nonetheless show that attention to that temperature dependence is necessary to explain differences between the physical parameters extracted from the C–V and I–V characteristics.

Given the similarity between Eqs. (2) and (15), Eq. (14) can be fitted to the experimental I–V data by the procedures described in Section 3.1. The resulting effective barrier height Φ_{ap} and ideality factor n_{ap} should obey Eqs. (16) and (17). The plot of Φ_{ap} as a function of 1/2kT ought to be a straight line, the intercept and slope of which determine the Gaussian parameters $\overline{\Phi}_{bo}$ and σ_o, respectively. Figure 8 applies this procedure to our data, linear regression yielding $\overline{\Phi}_{bo} = 0.90$ eV and $\sigma_o = 0.0135$ V, respectively. From the intercept and slope of the plot of n_{ap} as a function of 1/2kT, we obtain the voltage coefficients $\rho_2 = 0.156$ V and $\rho_3 = 0.149$ V, respectively.

The standard deviation gauges the barrier homogeneity. Since $\sigma_o = 0.149$ eV is not small in comparison with the mean value $\overline{\Phi}_{bo} = 0.90$ eV, we conclude that the interface is significantly inhomogeneous. The potential fluctuations associated with the inhomogeneity affect the low-temperature I–V characteristics and in particular account for the curved Richardson plots.

To account for the barrier inhomogeneities, Richardson's procedure must therefore be generalized. With this in mind, we combine Eqs. (15) and (16) and write down the equality:

$$\ln\left(\frac{I_o}{T^2}\right) - \left(\frac{q^2\sigma_o^2}{2k^2T^2}\right) = \ln(AA^*) - \frac{q\overline{\Phi}_{bo}}{kT} \tag{18}$$

which reduces to Eq. (4) in the limit $\sigma_o \to 0$.

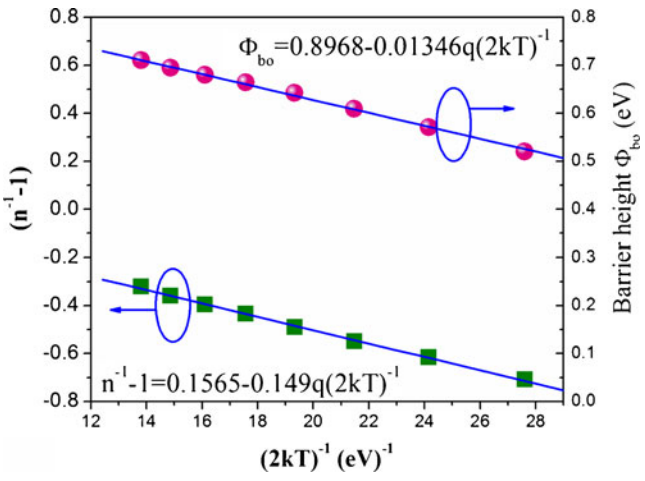

Fig. 8 The apparent barrier height Φ_{ap} (*closed circles*) obtained from I–V measurements as a function of inverse temperature and inverse ideality factor $1/n_{ap}$ (*closed squares*) versus inverse temperature plots for Ni/Cu/n-InP SBDs

In the conventional Richardson plot, $\ln(I_o/T^2)$ is shown as a function of 10^3/T. Equation (18) defines the modified Richardson plot, which depicts $\ln(I_o/T^2) - q^2\sigma_o^2/2(kT)^2$ as a function of 10^3/T. A straight line is expected, the slope and the intercept of which yield the mean $\overline{\Phi}_{bo}$ and Richardson's constant A^*. Figure 9 shows $\ln(I_o/T^2) - q^2\sigma_o^2/2(kT)^2$ as a function of 10^3/T for our data, from which we obtain $\overline{\Phi}_{bo} = 0.89$ eV and $A^* = 6.54$ A/(cm K)^2, respectively, with no reference to the temperature coefficients of the barrier height. The result $\overline{\Phi}_{bo} = 0.89$ eV is in good agreement with $\overline{\Phi}_{bo} = 0.90$ eV, obtained from Fig. 8, and the Richardson constant $A^* = 6.54$ A/(cm K)^2 is much closer to the theoretical prediction $A^* = 9.4$ A/(cm K)^2 for n-type InP than the result $A^* = 3.7 \times 10^{-3}$ A/(cm K)^2 from Eq. (4).

3.3 Capacitance–Voltage Characteristics

To analyze the experimental C–V characteristics have employed the Schottky–Mott equation [9]

$$C = \sqrt{\frac{q\varepsilon_S N_d A^2}{2(V_{bi} - V - V_T)}}, \tag{19}$$

where ε_S is the semiconductor dielectric constant, A is the area of the Schottky diode, N_d is the concentration of ionized donor atoms, V_{bi} is the built-in potential, V_T(=kT/q) is a thermal voltage, and V is the applied reverse bias. Equation (19) yields the following expression for donor concentration:

$$N_d = \frac{2}{q\varepsilon_S A^2}\left[-\frac{1}{(d(1/C^2)/dV)}\right] \tag{20}$$

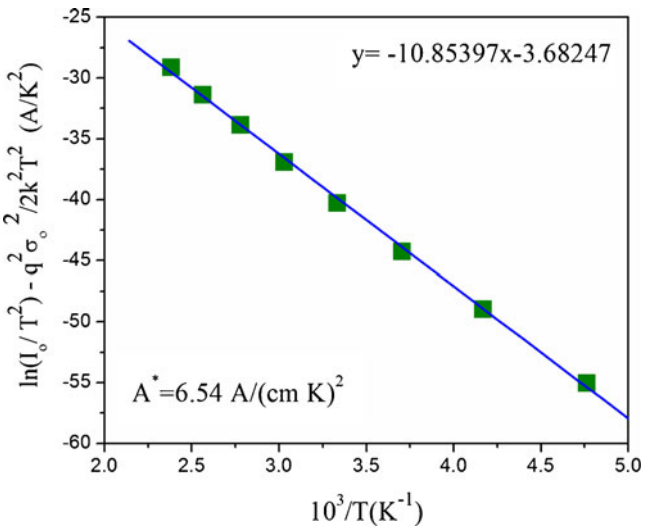

Fig. 9 Modified Richardson plot, $\ln(I_o/T^2) - q^2\sigma_o^2/2(kT)^2$ versus 10^3/T, and its linear fit for the Ni/Cu/n-InP SBD according to a Gaussian distribution of the barrier heights

which determines the ionized donor concentration from the slope of $1/C^2$ vs. V curve. The SBH $\Phi_{bo}{}^{C-V}$ is related to the built-in voltage V_{bi} by the following equation:

$$\Phi_{bo}^{C-V} = V_{bi} + \frac{kT}{q}\ln\left(\frac{N_C}{N_d}\right) \tag{21}$$

with

$$N_C = 2\left(\frac{(2m^* kT)^{3/2}}{h^3}\right) \tag{22}$$

where N_C is the effective density of states in the InP conduction band and $m^*=0.078m_0$ is the effective electronic mass in InP [9].

The voltage-axis intercept of the $1/C^2$ versus V curve determines the built-in potential V_{bi}. Figure 10 displays $1/C^2$ as a function of V for our Ni/Cu/n-InP SBD in the temperature range 210–420 K, the junction capacitance being measured at 1 MHz. The plots are linear because the interface states and the inversion layer charge cannot follow the AC signal at 1 MHz and therefore make negligible contributions to the diode capacitance. In the 0.0 to −2.0 V range the capacitance grows with temperature. The donor concentration computed from Eq. (20) is shown in Fig. 11 as a function of temperature. The concentration grow monotonically with temperature from $N_d=1.78\times10^{15}$ at 210 K to $N_d=3.34\times10^{15}$ cm^{-3} at 420 K.

The measured SBHs, which decrease from $\Phi_{bo}^{C-V}=0.78$ eV at 210 K to $\Phi_{bo}^{C-V}=0.63$ eV at 420 K, are listed in Table 2 along with the barrier heights extracted from the I–V characteristics. In the same way that it describes the strong temperature dependences of $\Phi_{bo}{}^{I-V}$ and n at low T, the assumption of a Gaussian distribution of barrier heights, i.e., Eq. (12), explains the differences between $\Phi_{bo}{}^{I-V}$ and $\Phi_{bo}{}^{C-V}$. The capacitance is insensitive to the standard deviation σ_o of the barrier distribution and therefore centrally

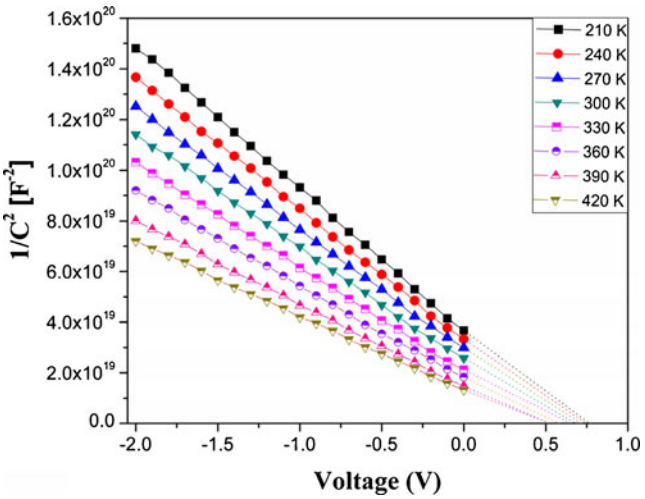

Fig. 10 Experimental C^{-2}–V characteristics of a typical Ni/Cu/n-InP SBDs in the temperature range of 210–420 K

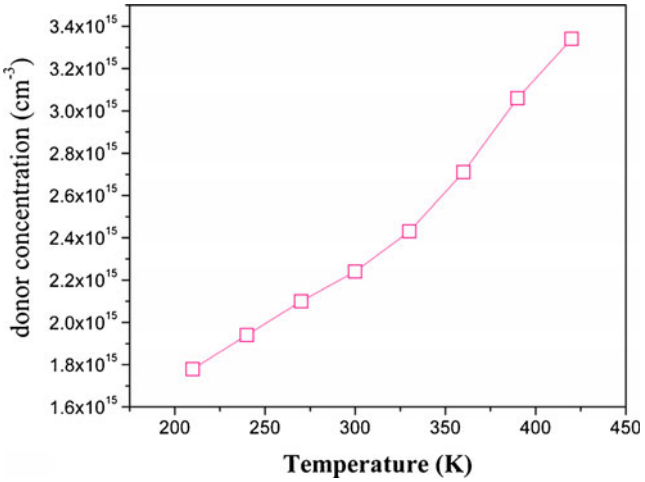

Fig. 11 Variation of donor concentration (N_d) with temperature of Ni/Cu/n-InP SBD attained from reverse bias C^{-2}–V characteristics

determined by the mean band bending in the Schottky barrier [14]. Since the currents are sensitive to the deviation, differences arises, from which one can extract information on σ_o. To this end, we assume that the square of the deviation varies linearly with temperature, i.e., that $\sigma^2=\sigma_o{}^2-\alpha_\sigma T$, where both σ_o and α_σ are empirical distribution parameters that must be extracted from the experimental data. The difference between the barrier heights from the C–V and I–V characteristics is then expressed by the following equality [14]:

$$\Phi_{bo}^{C-V} - \Phi_{bo}^{I-V} = -\frac{q\sigma_o^2}{2kT} + \frac{q\alpha_\sigma}{2k} \tag{23}$$

Figure 12 plots $\left(\Phi_{bo}^{C-V} - \Phi_{bo}^{I-V}\right)$ as a function of $(2kT)^{-1}$. According to Eq. (23), the slope of the resulting straight line is $\sigma_o^2/2k$, and the y-axis intercept is $\alpha_\sigma/2k$, which determine the parameters σ_o and α_σ. We find $\sigma_o=0.152$ eV and $\alpha_\sigma=$

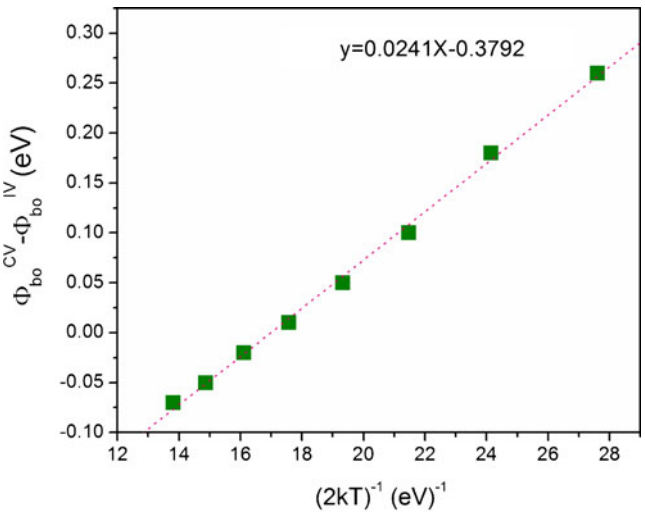

Fig. 12 The experimental $\left(\Phi_{bo}^{C-V} - \Phi_{bo}^{I-V}\right)$ versus $(2kT)^{-1}$ plot of the Ni/Cu/n-InP SBD according to Gaussian distribution of barrier heights

4.56×10^{-5} V^2 K^{-1}, the former in close agreement with the result σ_o=0.149 eV from the plot of Φ_{bo} versus $(2kT)^{-1}$ in Fig. 8 interpreted according to Eq. (16). The agreement between the two independently computed deviations confirms that relatively strong potential fluctuations affect the I–V curves at low temperature making the conventional Richardson plot in Fig. 3 nonlinear.

To better understand the origin of such fluctuations, we are currently studying the effects of annealing on the electrical and structural properties of Ni/Cu Schottky contacts to InP and plan to present results in a future report.

4 Conclusions

We have measured the I–V and C–V characteristics of Ni/Cu/n-InP SBDs at eight uniformly spaced temperatures in the 210–420 K range. On the basis of the TE model, we found the I–V barrier heights to grow from 0.52 to 0.70 eV, while the ideality factor decayed from 3.31 to 1.47 upon heating in that temperature interval. The series resistances calculated by Cheung's and Norde's procedures were found to decrease upon heating. The thermal dependence of the measured barrier height and ideality factor was shown to be consistent with a Gaussian distribution of barrier heights, an indication that the barrier potential is spatially variable. An effective Richardson constant A^*=6.54 A/(cm K)^2 was obtained from a Richardson plot modified to account for the barrier inhomogeneity, a result that roughly agrees with the theoretical value A^*= 9.4 A/(cm K)^2. The standard deviations of the distribution computed (1) directly from the thermal dependence of the I–V characteristics and (2) from the thermal dependence of the difference between barrier heights obtained from the I–V and C–V characteristics showed very good agreement. We conclude that the physics of conduction in Ni/Cu/n-InP Schottky barrier diodes is governed by thermal activation, mathematically described by thermionic emission theory. The seemingly anomalous thermal dependence of the I–V characteristics is due to spatial inhomogeneity within the Schottky barriers.

Acknowledgments This work was supported by Kyungpook National University Research Fund 2012, 2008 Brain Korea 21 (BK21), the National Research Foundation of Korea grants funded by MEST (2012–0005671, 2012–0000627), R&D program of MKE/KETEP (2011101050017B), WCU (World Class University) program (grant R33-10055) and IT R&D program of MKE/KEIT (10038766), and the IT R&D program of MKE/KEIT (10038766).

References

1. P.M. Smith, P.C. Chao, K.H.G. Duh, L.F. Lester, B.R. Lee, Electron. Lett. **22**, 781 (1986)
2. S.Y. Wang, S.H. Lin, Y.M. Huang, Appl. Phys. Lett. **51**, 83 (1987)
3. M. Razeghi, R. Blondeau, M. Krakowski, B. de Cremoux, J.P. Duchemin, F. Lozes, M. Martinot, M.A. Bensoussan, Appl. Phys. Lett. **50**, 230 (1987)
4. H.C. Card, E.H. Rhoderick, J. Phys. D: Appl. Phys. **7**, 1589 (1971)
5. P.G. McCafferty, A. Sellai, P. Dawson, H. Elabd, Solid-State Electron. **39**, 583 (1996)
6. S. Chand, J. Kumar, Appl. Phys. A. **65**, 497 (1996)
7. E.H. Rhoderick, R.H. Williams, *Metal–semiconductor contacts* (Clarendon, Oxford, 1978)
8. L. Rideout, Thin Solid Films **48**, 261 (1978)
9. S.M. Sze, *Physics of semiconductor devices*, 2nd edn. (Wiley, New York, 1981)
10. Z. Horvath, J. Appl. Phys. **63**, 976 (1988)
11. J.H. Werner, H.H. Guttler, J. Appl. Phys. **69**, 1522 (1991)
12. R.T. Tung, Phys. Rev. B **45**, 13504 (1992)
13. S. Chand, J. Kumar, J. Appl. Phys. **82**, 5005 (1997)
14. J.H. Werner, H.H. Guttler, J. Appl. Phys. **73**, 1315 (1993)
15. Y.P. Song, R.L. Van Meirhaeghe, W.H. Laflere, F. Cardon, Solid-State Electron. **29**, 633 (1986)
16. A. Gumus, A. Trust, N. Yalcin, J. Appl. Phys. **91**, 245 (2002)
17. I. Dokme, S. Altindal, Semicond. Sci. Technol. **21**, 1053 (2006)
18. E. Dobrocka, J. Osvald, Appl. Phys. Lett. **65**, 575 (1994)
19. P.P. Hankare, P.A. Chate, P.V. Chavan, D.J. Sahte, J. Alloys Compd. **461**, 623 (2008)
20. M.M. El-Nahass, K.F. Abd El-Rahman, J. Alloys Compd. **430**, 194 (2007)
21. K. Akkilic, F. Yakuphanoglu, Microelectron. Eng. **85**, 1826 (2008)
22. H. Cetin, E. Ayyildiz, Semicond. Sci. Technol. **20**, 625 (2005)
23. F.E. Cimilli, H. Efeoglu, M. Saglam, A. Turut, J. Mater. Sci. Mater. Electron. **20**, 105 (2009)
24. M. Soylu, B. Abay, Microelectron. Eng. **86**, 88 (2009)
25. S. Shankar Naik, V. Rajagopal Reddy, Superlattice. Microstruct. **48**, 330 (2010)
26. D. Subba Reddy, M. Siva Pratap Reddy, V. Rajagopal Reddy, Optoelectron. Adv. Mater. Rapid Commun. **5**, 448 (2011)
27. S. Chand, J. Kumar, J. Appl. Phys. **80**, 288 (1996)
28. S. Zhu, C. Detavernier, R.L. Van Meirhaeghe, F. Cardon, G.P. Ru, X.P. Qu, B.Z. Li, Solid-State Electron. **44**, 1807 (2000)
29. S. Bandyopadhyay, A. Battacharyya, S.K. Sen, J. Appl. Phys. **85**, 3671 (1999)
30. Z.J. Horvath, Solid-State Electron. **39**, 176 (1996)
31. R.F. Schmitsdrof, T.U. Kampen, W. Monch, J. Vac. Technol. B **15**, 1221 (1997)
32. R.F. Schmitsdrof, T.U. Kampen, W. Monch, Surf. Sci. **324**, 249 (1997)
33. S.K. Cheung, N.W. Cheung, Appl. Phys. Lett. **49**, 85 (1986)
34. M. Saglam, A. Ates, B. Guzeldir, A. Astam, M.A. Yildirim, J. Alloys Compd. **184**, 570 (2009)
35. H. Norde, J. Appl. Phys. **50**, 5052 (1979)
36. V.W.L. Chin, M.A. Green, J.W.V. Storey, J. Appl. Phys. **68**, 3470 (1990)
37. S. Chand, J. Kumar, Appl. Phys. A **63**, 171 (1996)